# High Thermopower with Metallic Conductivity in $p$-Type Li-Substituted $PbPdO_2$

Leo K. Lamontagne,[†,‡] Geneva Laurita,[‡] Michael W. Gaultois,[¶,‡] Michael Knight,[‡] Leila Ghadbeigi,[§] Taylor D. Sparks,[§] Markus E. Gruner,[∥] Rossitza Pentcheva,[∥] Craig M. Brown,[⊥] and Ram Seshadri[*,‡,†,¶]

†*Materials Department, University of California, Santa Barbara, CA 93106*

‡*Materials Research Laboratory, University of California, Santa Barbara, CA 93106*

¶*Department of Chemistry and Biochemistry, University of California, Santa Barbara, CA 93106*

§*Department of Materials Science and Engineering, University of Utah, Salt Lake City, UT 84112*

∥*Department of Physics and Center for Nanointegration Duisburg-Essen (CENIDE) University of Duisburg-Essen, Lotharstr. 1, 47057 Duisburg, Germany*

⊥*Center for Neutron Research, National Institute of Standards and Technology, Gaithersburg, MD 20899*

E-mail: seshadri@mrl.ucsb.edu

**Abstract**

$PbPdO_2$ is a band semiconductor with a band gap arising from the filled $d^8$ nature of square-planar $Pd^{2+}$. We establish that hole doping through Li substitution for Pd in $PbPdO_2$ results in a $p$-type metallic oxide with a positive temperature coefficient of resistance for substitution amounts as small as 2 mol % of Li for Pd. Furthermore, $PbPd_{1-x}Li_xO_2$ demonstrates a high Seebeck coefficient, and is therefore an oxide thermoelectric material with high thermopower despite the metallic conductivity. Up to 4 mol % Li is found to substitute for Pd as verified by Rietveld refinement of neutron diffraction data. At this maximum Li-substitution, the resistivity is driven below the Mott metallic maximum to $3.5\times10^{-3}\,\Omega\,$cm with a Seebeck coefficient of 115 $\mu$V/K at room temperature which increases to 175 $\mu$V/K at 600 K. These electrical properties are almost identical to the well-known $p$-type oxide thermoelectric $Na_xCoO_2$. Non-magnetic Li-substituted $PbPdO_2$ does not possess a correlated, magnetic state with high spin degeneracy as found in some complex cobalt oxides. This suggests that there are other avenues to achieving high Seebeck coefficients with metallic conductivities in oxide thermoelectrics. The electrical properties coupled with the moderately low lattice thermal conductivities allow for a $zT = 0.12$ at 600 K; the maximum temperature measured here. The trend suggests yet higher values at elevated temperatures. First-principles calculations of the electronic structure and electrical transport provide insight into the observed properties.

# Introduction

Thermoelectric materials develop an electrical potential when subject to a temperature gradient owing to the Seebeck effect, and conversely develop a thermal gradient when subject to an electrical potential through the Peltier effect. Devices made from such thermoelectric materials are currently used for refrigeration and heating, and are being widely explored for waste heat recovery.[1] To be effective, these materials must have low electrical resistivities to conduct the charge carriers with minimal loss, and a high Seebeck coefficient to produce sufficient voltages. Additionally they should have minimal lattice thermal conductivity, since the thermal gradient must be maintained. These properties combine in a dimensionless thermoelectric figure of merit $zT$ given by the formula $zT = S^2T/(\rho\kappa)$, where $S$ is the Seebeck coefficient, $\rho$ is the electrical resistivity, and $\kappa$ the total thermal conductivity, measured at temperature $T$. In addition to their utility, thermoelectric measurements provide deep insights into the electrical and thermal transport properties of materials, including insight into the underlying band structure.

Oxide materials possess many attractive qualities for waste heat recovery as they are generally light weight materials with the potential for high temperature air stability.[2,3] However, oxide materials have not reached the level of performance of current state-of-the-art main group thermoelectrics. This is in part due to higher thermal conductivities compared to other material families, but is additionally a result of low power factors ($S^2/\rho$). While many oxides possess favorable Seebeck coefficients, finding oxides with the necessary metallic conductivities while retaining these high Seebeck coefficients has proved difficult.[4] Currently, the highest performing oxide materials are $p$-type complex cobalt oxides which sprung from the discovery of high thermopower in metallic $Na_xCoO_2$.[5] These compounds possess metallic resistivities yet retain high Seebeck coefficients. A key feature in all of the promising cobalt oxides are $CoO_2$ layers comprising mixed valent $Co^{3+}$ and $Co^{4+}$. The highly correlated, mixed valent cobalt ions provide the necessary electrical properties, and the layered structure results in a low thermal conductivity, giving rise to a

modestly high thermoelectric performance.

With the promising performance of the complex cobalt oxides, research into the thermoelectric properties of other oxide materials has been of interest. Misfit rhodium oxides have been explored as the 4$d$ analogues of the cobalt oxides and have shown comparable room temperature Seebeck coefficients with metallic conductivities.[6–8] However, the exploration of other 4$d$ metal compounds has been relatively sparse.

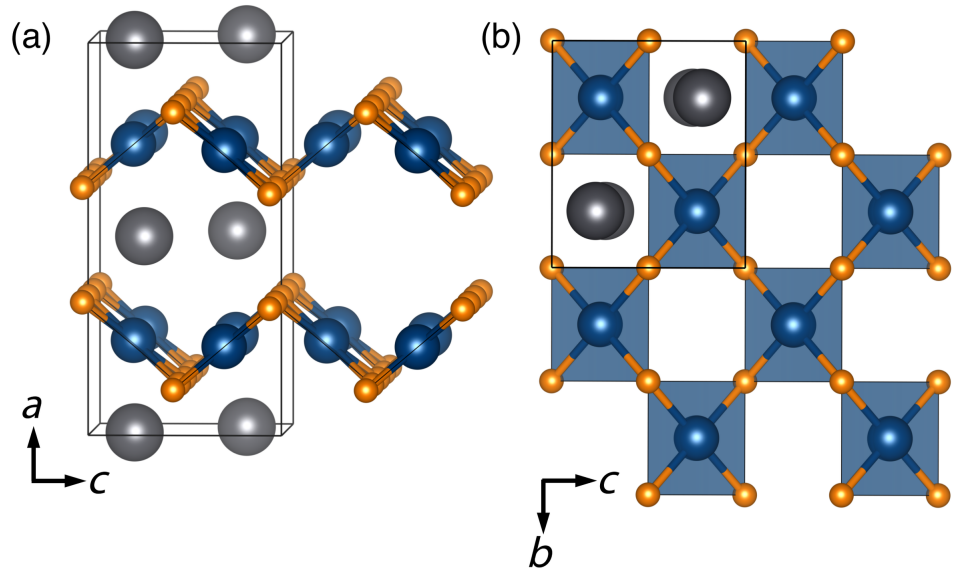


Figure 1: Depictions of the orthorhombic $Imma$ (space group #74) crystal structures of $PbPdO_2$. (a) Shows the corrugated layers of corner-connected $PdO_4$ square planes, arranged in a checkerboard pattern as seen in the top view in (b). Pb atoms (large spheres) are 4-coordinate with O, capping $PbO_4$ square pyramids between the Pd–O layers.

Complex oxides of palladium are particularly interesting as many are known to undergo compositionally driven metal-insulator transitions with hole doping,[9,10] and the transitional regime is often a fertile playground for thermoelectric research. PdO itself is driven metallic with as little as 1 mol % Li substitution.[11] $p$-type oxide metals starting from non-magnetic parent compounds are relatively uncommon, prompting the investigation of their thermoelectric properties. $PbPdO_2$ is an attractive material for thermoelectric investigation due to its layered nature of Pd square planar units (suggesting potentially lower thermal conductivity) and the possibility for hole doping (suggesting control of elec-

trical properties). $PbPdO_2$, like many other complex palladium oxides, is a small band gap semiconductor. Below 100 K, the resistivity has been reported to display semiconducting behavior *ie.* it increases with decreasing temperature. Above 100 K, the material behaves like a metal with resistivity increasing with temperature.[12] The structure shown in Figure 1 consists of layers of Pb atoms, with the lone pairs pointing in the plane, alternating with layers of square planar $PdO_4$ units. These $PdO_4$ square planes form a two dimensional tilted checkerboard pattern.[13] $PbPdO_2$ has attracted attention following suggestions from preliminary electronic structure calculations that it could behave potentially as a spin gapless semiconductor with appropriate substitution.[14,15] More recent calculations using hybrid functionals have pointed to the existence of a small band gap.[16] $PbPdO_2$ has been shown previously to incorporate Co[17,18] and Cu[19] onto the Pd site. The small band gap and potential to control electrical properties through aliovalent substitution, coupled with an interesting layered structure, makes it attractive for exploring thermoelectric properties.

Here we report the thermoelectric performance of polycrystalline Li-substituted $PbPdO_2$ at elevated temperatures. Rietveld refinements of neutron diffraction patterns confirm the Li substitution onto the Pd site, with a solubility limit of approximately 4 mol % Li. With Li-substitution, we observe a 10-fold decrease in the resistivity to below the Mott metallic limit without a precipitous drop in the Seebeck coefficient. Metallic conductivities with Seebeck coefficients nearing 200 $\mu$V/K at 600 K are remarkable in a non-magnetic oxide material, and points to the need to explore other oxide systems for thermoelectric performance. The experimental results are backed up with density functional theory electronic structure calculations, including calculations of the Seebeck coefficient within Boltzmann transport theory, which suggest that the unusually high power factor is likely to have its origins in the unusual band structure, rather than as a result of spin or charge correlation.

# Methods

Polycrystalline samples of $PbPdO_2$ without and with Li substituting for Pd were prepared by heating stoichiometric amounts of $PbCO_3$, PdO, and $Li_2CO_3$ powders. The precursors were finely ground using an agate mortar and pestle and pressed into pellets at 100 MPa. The pellets were placed on beds of powder of the same composition to prevent contamination from the alumina crucible. Reactions were carried out at 700 °C for 12 hours. Samples were reground and reheated several times (typically three times) to ensure a complete reaction of the precursors.

Laboratory X-ray diffraction studies were carried out on samples mixed with a silicon standard on a Panalytical Empyrean diffractometer with Cu-$K_\alpha$ radiation. Neutron diffraction studies on samples loaded in vanadium cans at room temperature employed a constant $\lambda = 2.078$ Å wavelength from a Ge-(311) monochromator of the BT-1 neutron powder diffractometer at the National Institute for Standards and Technology (NIST). Neutron powder diffraction was carried out on the stoichiometric and the highest Li-substituted sample. Rietveld[20] refinement was performed using the TOPAS academic software suite.[21] Crystal structures were visualized using VESTA.[22] Prior to the measurement of physical properties, the resulting powders were compacted into dense pellets using Spark Plasma Sintering (SPS), following details described previously.[23] Densification was carried out at $T$ = 950 K, as measured by a pyrometer, for 15 minutes under vacuum, with residual Ar flow. Neutron diffraction measurements carried out before and after the SPS treatment did not reveal any significant changes in the structure and composition. Pycnometry measurements conducted on a Micromeritics AccuPyc 1340 Pycnometer confirm sample densities greater than 95% of the theoretical density for all samples. Elemental analysis was performed on the stoichiometric and highest substituted samples by Galbraith Laboratories, Knoxville TN. For the nominal composition $PbPdO_2$, the analysis gave Pb:Pd

Certain commercial equipment, instruments, or materials are identified in this document. Such identification does not imply recommendation or endorsement by the National Institute of Standards and Technology nor does it imply that the products identified are necessarily the best.

weight ratio of 60.9%:28.0 (expected 59.9%:30.8%) and for the nominal 8 mol % Li-substituted sample, the analysis gave a Pb:Pd:Li ratio of 59.7%:26.5%:0.168% (expected 61.3%29.0%:0.164%). The Seebeck coefficient and electrical resistivity were measured in a He atmosphere under-pressure using an ULVAC Technologies ZEM-3 instrument. Hall coefficients were measured at 11 K using a 4 probe configuration on a Quantum Design Dynacool PPMS. Thermal diffusivity was measured using the laser flash technique between room temperature and 973 K under an air atmosphere on a Netzsch LFA 457 system. Pellets for the measurement, approximately 8 mm in diameter and 2 mm thick, were sprayed with a layer of carbon paint in order to minimize errors in the emissivity. The thermal conductivity was calculated using $\kappa = \alpha C_{\mathrm{p}} \rho$, where $\alpha$, $C_{\mathrm{p}}$, and $\rho$ are thermal diffusivity, heat capacity, and density, respectively. The Cowan model[24] for determining diffusivity, and the Dulong-Petit molar heat capacity, $C_{\mathrm{p}} = 3R$, were employed.

The electronic structure of unsubstituted $PbPdO_2$ was calculated using density functional theory (DFT) as implemented in the Vienna *ab initio* Simulation Package VASP[25,26] with projector-augmented wave (PAW) pseudopotentials.[27,28] A cut-off energy of 500 eV was employed, which is substantially above the requirements for the potentials and scalar-relativistic corrections. For structure optimization and band structure calculations, the Perdew-Burke-Ernzerhof exchange-correlation functional within the generalized gradient approximation (GGA-PBE) was employed.[29] The standard primitive unit cell of the conventional body-centered orthorhombic cell was obtained using AFLOW.[30] A $\Gamma$ centered $k$-mesh of 8×8×8 was used for structure optimization. The Brillouin zone paths for band structure calculations were adapted from Setyawan and Curtarolo.[31] Additional calculations of the density of states (DOS) employed the HSE06 screened hybrid functional.[32] Spin-orbit coupling (SOC) can be important for empty $Pb^{2+}$ $6p$ states.[33] Calculations of the band structure with and without spin-orbit coupling verified that valence band states, which are the important consideration here, are not impacted by the exclusion of SOC. Transport properties were calculated at constant carrier concentration using Boltzmann transport theory in the

constant relaxation time approximation. We employed the BOLTZTRAP code[34] based on $k$-dependent eigenvalues obtained from DFT calculations performed with VASP. Further details of how such calculations were carried out are provided alongside the results of the calculations.

# Results and discussion

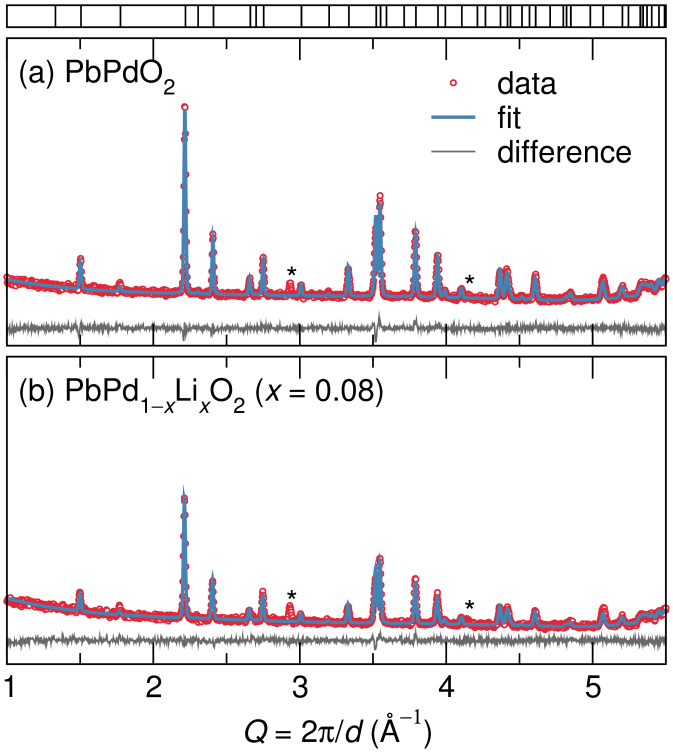


Figure 2: Rietveld refinements of neutron diffraction data of (a) pristine $PbPdO_2$ and (b) the nominally 8 mol %-substituted $PbPd_{0.92}Li_{0.08}O_2$, showing the quality of the fits. The top panel indicates the Bragg reflection marks for $PbPdO_2$. Asterisks mark the positions of reflections from the vanadium sample can.

## Preparation and characterization

Various amounts of Li were substituted into $PbPdO_2$ to study the change in electronic properties. $Li^+$ was expected to substitute for $Pd^{2+}$ rather than $Pb^{2+}$ because of their similar

Shannon-Prewitt ionic radii: 0.590 Å for 4-coordinate $Li^{+}$, 0.64 Å for 4-coordinate square planar $Pd^{2+}$, and 0.98 Å for 4-coordinate $Pb^{2+}$.[35] Rietveld refinement of neutron diffraction patterns was performed to confirm the location and amount of Li substitution into the structure as Li poorly scatters X-rays. The samples studied here are post-SPS, and represent the materials whose physical properties were measured. Figure 2 shows the Rietveld refinements of both (a) the stoichiometric $PbPdO_2$, and (b) the nominally substituted $PbPd_{0.92}Li_{0.08}O_2$; the results of which are summarized in Table 1. The Li occupancy on the Pd site for the nominally 8 mol %-substituted sample was determined to be 4.2(9)%. The Pd and Li occupancy was constrained to sum to 1. The excess Li is not observed in neutron diffraction, though elemental analysis matches the nominal Li content. The Li impurity phase is most likely too small to see in diffraction data. Refinements with the Li on the Pb site were conducted, but did not improve the fits, supporting the Li substitution on the Pd site.

In further support for Li substitution for the Pd, the bond valence sums (BVS) for Li on both the Pd and Pb sites were calculated.[36] Li on the Pd site with a Li–O bond distance of 2.029 Å gives a BVS = 0.87. On the Pb site, the Li–O distance is 2.339 Å, giving a BVS = 0.38. While both sites leave Li underbonded, Li on the Pd site is more favored as the BVS is closer to the ideal value of BVS = 1 for $Li^{+}$.

For the nominally 8 mol % Li substitution, PbO impurities were observed by diffraction prior to SPS. No PbO phase is observed after SPS possibly due to the reducing atmosphere of the SPS process which can result in Pb being reduced and melted into the graphite die. In addition to densifying the material, SPS appears to introduce approximately 6 % Pb vacancies in the samples, while no oxygen vacancies were observed.

The change of the lattice parameters with Li substitution was monitored to further understand structural and compositional changes. Figure 3 shows the room temperature resistivity, lattice parameters and unit cell volume as a function of substitution. The room temperature resistivity drops below the Mott metallic limit of $10^{-2}\,\Omega\,$cm with as little 2 %

Table 1: Structural parameters of $PbPdO_2$ at room temperature, as determined by Rietveld refinement of neutron diffraction data. Orthorhombic space group: $Imma$ (#74) The sites are Pb 4$e$ $(0, \frac{1}{4}, z)$; Pd 4$c$ $(\frac{1}{4}, \frac{1}{4}, \frac{1}{4})$, and O 8$f$$(x, 0, 0)$.

| Nominal Composition | $PbPdO_2$ | $PbPd_{0.92}Li_{0.08}O_2$ |
|---|---|---|
| $a$ (Å) | 9.4394(4) | 9.4358(6) |
| $b$ (Å) | 5.4508(2) | 5.4487(3) |
| $c$ (Å) | 4.6514(2) | 4.6470(3) |
| Pb Occupancy | 0.94(1) | 0.927(9) |
| Li Occupancy | – | 0.042(9) |
| Pb $z$ Position | 0.7751(6) | 0.780(7) |
| O $x$ Position | 0.3488(4) | 0.3498(5) |
| Pb $U_{iso}$ (Å$^2$) | 0.010(1) | 0.012(1) |
| Pd/Li $U_{iso}$ (Å$^2$) | 0.005(2) | 0.004(2) |
| O $U_{iso}$ (Å$^2$) | 0.010(1) | 0.014(1) |
| O–O–O (°) | 102.5(2) | 101.9(3) |
| $R_{wp}$ (%) | 3.9 | 3.5 |

Li substitution and only decreases slightly with further substitution. Upon substitution, the $a$ and $b$ lattice parameters remain relatively constant, while the $c$ axis contracts with Li content up to 4 mol % Li. A lattice contraction is expected due to the smaller Li ion as well as the necessary oxidation of $Pd^{2+}$ to $Pd^{3+}$ to maintain neutrality. The $c$ lattice parameter remains constant after 4 % Li substitution, which suggests a solubility limit of Li into the structure further supporting the refined Li occupancy values from neutron diffraction of the nominal 8 mol % sample. This also explains the PbO impurity phase in the higher-substituted samples. The small solubility limit of Li potentially arises from steric resistance to further lattice contraction from the Pb lone pairs, and resistance of Pd to further oxidize.

Ozawa *et al.* have reported that the angle of the Pd square planes can affect the electrical properties.[19] The difference in this angle with Li substitution (O–O–O(°) in Table 1) is only 0.6 °. Thus, a slight change in orbital overlap is not likely to significantly affect the electrical properties relative to the increased charge carriers from hole-doping.

## Electrical transport and Seebeck coefficient

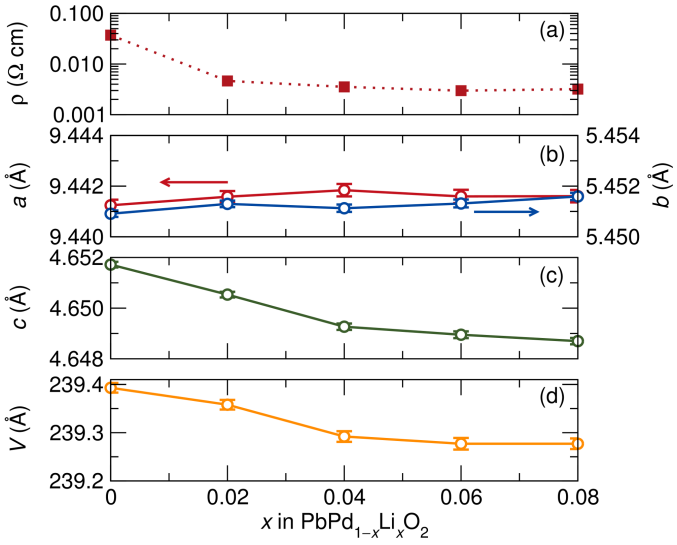


Figure 3: Room temperature resistivity, lattice parameter and unit cell volume changes as a function of Li substitution in $PbPdO_2$. Only the $c$ parameter changes significantly up to 4 mol % Li. The constant values above 4 mol % suggest a solubility limit of Li in the structure. Error bars indicate one standard deviation.

The electrical properties of $PbPdO_2$ with substitution are shown in Figure 4. Stoichiometric $PbPdO_2$ shows a room temperature resistivity of 0.037 Ω cm, which is considerably lower than the 0.75 Ω cm reported by Ozawa and co-workers.[12] The difference can be attributed to the densification of the material through SPS. Upon substitution with 4 mol % Li, the room temperature resistivity drops to $3.5\times10^{-3}$ Ω cm. The Seebeck coefficient is 215 $\mu$V/K at room temperature for $PbPdO_2$. This is also substantially higher than previous reports, possibly due to densification from SPS. It is unusual for both the resistivity and Seebeck coefficient to change favorably, highlighting the importance of dense pellets not only for their robustness, but also for optimal performance. Upon substitution with Li, the Seebeck coefficient drops, but the room temperature value is still greater than 100 $\mu$V/K for all substitutions and increases with temperature. Because of instrumental constraints requiring a He atmosphere for sample measurements, it was not possible to reliably measure samples at higher temperatures due to surface reduction. Therefore, peak Seebeck coefficients are not reached for the temperatures measured and approach 200 $\mu$V/K at

600 K. However, the materials are stable in air to temperatures of 1000 K at which even higher Seebeck coefficients would be expected.

Hall measurements on the stoichiometric and 8 mol % Li substituted samples suggested carrier concentrations of $1.88\times10^{18}$ cm$^{-3}$ and $3.72\times10^{18}$ cm$^{-3}$ respectively. These concentrations are an order of magnitude higher than the the value of $1.8\times10^{17}$ cm$^{-3}$ reported by Ozawa and co-workers[12] which in turn explains why we observe an order of magnitude difference in resistivity (lower in the samples measured here). It is expected, that given an order of magnitude decrease in the resistivity with Li substitution, we would see a corresponding increase in the carrier concentration. We see only a slight increase.

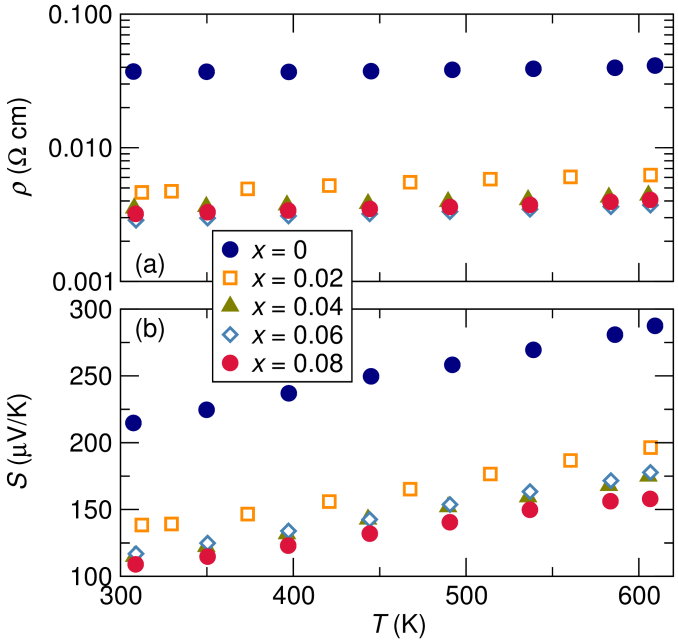


Figure 4: (a) Resistivity and (b) Seebeck coefficients for $PbPd_{1-x}Li_xO_2$. The resistivity drops by an order of magnitude with 2 mol % substitution while the Seebeck coefficient drops by 100 $\mu$V/K. The Seebeck coefficients of the Li-substituted samples increase with temperature and approach 200 $\mu$V/K at 600 K.

The resistivity and Seebeck coefficient values obtained for the polycrystalline Li-substituted $PbPdO_2$ materials are almost identical to those of polycrystalline $Na_xCoO_{2-\delta}$, which has a Seebeck coefficient of 100 $\mu$V/K and resistivity of $2\times10^{-3}\,\Omega$ cm at 300 K.[37] Single crystals of some complex cobalt oxides are the highest performing oxide thermo-

electric materials and many different compositions have been explored since the discovery of high thermopower in $NaCoO_2$.[38,39] Central to the thermoelectric performance of these cobaltate compounds is the high Seebeck coefficient with metallic resistivities. When first observed, the Heikes formula[40] was unable to explain the unexpected thermopower at high temperatures. Koshibae and co-workers proposed a generalized Heikes formula for these compounds which explained the high thermopower at elevated temperatures,[41,42] by accounting for the spin and orbital degeneracies associated with $Co^{3+}$ and $Co^{4+}$ in various spin states, supported by the observed reduction in the Seebeck with applied magnetic fields.[43] Other explanations point to unique band structures for this class of materials.[44–46]

Interestingly, Li-substituted $PbPdO_2$ consists of almost entirely diamagnetic square-planar, $Pd^{2+}$ except for the small number of holes that dope into the Pd–O conduction band. This implies that the relatively high Seebeck coefficient must arise for reasons distinct from what is observed in the complex cobalt oxides.

## Electronic structure and Boltzmann transport analysis

The electronic structure of $PbPdO_2$ was calculated to better understand the electronic properties and is shown in Figure 5. The GGA-PBE band structure suggests a semi-metal with the valence band maximum at the $Z$ point and the conduction band minimum at the $\Gamma$ point. On either side of the valence band maximum are flat regions that then disperse towards peaks at the $T$ and $Y$ points. The presence of both flat and disperse bands just under the Fermi level may explain the high Seebeck coefficient, in conjunction with moderately high mobility in the hole-doped compound. GGA-PBE is known to underestimate the band gap in $PbPbO_2$,[16] and leads to the semimetal prediction. In order to more reliably obtain the expected band gap of the material, hybrid functionals (HSE06) were employed to calculate the DOS.

Hybrid functionals such as HSE06,[32] which usually yield more realistic band gaps, were employed to obtain the densities of state of $PbPdO_2$, as shown in Figure 6(a). The calcu-

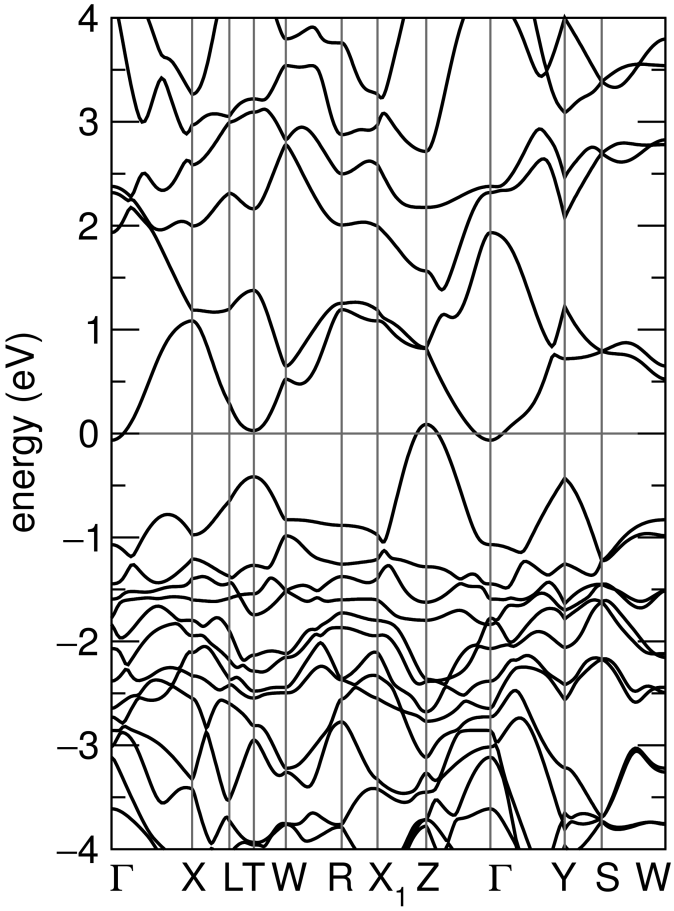


Figure 5: Band structure $PbPdO_2$ using the GGA-PBE functional, which predicts a semimetal with regions of flat and disperse bands below the Fermi level.

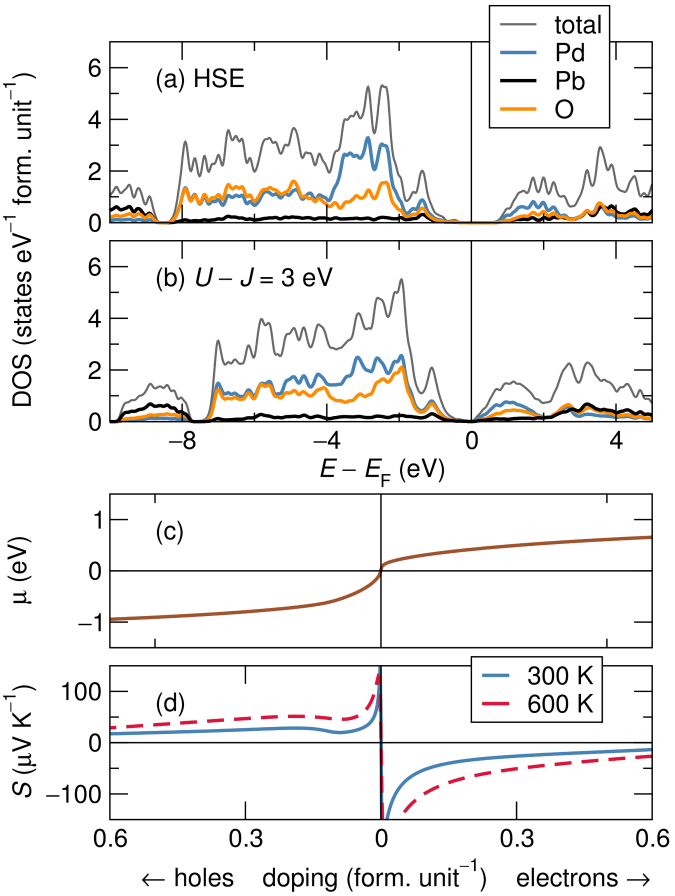


Figure 6: Element-resolved electronic density of states of $PbPdO_2$ from (a) HSE06 hybrid functional calculations and (b) GGA + $U$ calculations with $U_{eff}$ = 3 eV. The two bottom panels, (c) and (d) respectively display the chemical potential $\mu$ and the trace of the Seebeck coefficient tensor $S$ as a function of doping, as obtained from Boltzmann transport calculations.

lations employed 25% Hartree-Fock exchange. It is seen that the valence band comprises mostly Pd $d$ states and the filled O $p$ states, while the conduction band has components of Pd $d$ and Pb $s$ and $p$ states. Since a dense mesh of $k$-points are necessary to obtain acceptable accuracy for Boltzmann transport calculations, we did not continue with the computationally expensive HSE06 calculations, which were limited to a comparatively small $k$-point mesh of 83 in the full Brillouin zone. Instead, we used the GGA + $U$ scheme in the rotationally invariant scheme of Dudarev *et al.*,[47] where we invoked a Hubbard $U$ term on the Pd-$d$ states to correct for static correlations, using a value of $U$ between 2.65 eV and 5.65 eV. $J$ was fixed to 0.65 eV in both cases. Calculations of the band structure were carried out with and without SOC (which is computationally expensive) and it was verified that the valence band structure, which is of relevance to the hole-doping studied here, is largely unchanged upon ignoring SOC effects, and SOC was not employed for the transport calculations. The computationally simpler scheme allowed us to employ $31^3$ $k$-points (*ie.* 29791 $k$-points) in the full Brillouin zone which, in combination with the standard settings for BOLTZTRAP, provided sufficiently converged transport properties in the prior, similar case of $PtCoO_2$.[48] Starting approximately from $U_{eff} = U - J = 3$ eV, a band gap opens that is significantly smaller than the gap obtained with the hybrid functional as seen in Figure 6(b). However, the absolute position of the peaks, the overall shape of the DOS, and character and hybridization of states are rather similar for the valence band, for the HSE06 calculation and for the $U_{eff} = U - J = 3$ eV, calculation.

Panels (c) and (d) of Figure 6 respectively display the chemical potential $\mu$ and the trace of the Seebeck coefficient tensor, as a function of filling in terms of doping of holes or electrons *per* formula unit, as obtained from the Boltzmann transport calculations. As one removes electrons from $PbPdO_2$ and dopes holes into the valence band, it is seen that the chemical potential does not change very much, even for quite substantial doping [Figure 6(c)]. The Seebeck coefficient was seen to be somewhat isotropic, and therefore only the trace of the Seebeck tensor $S$ is displayed here. $S$ is seen to rapidly drop just as one

introduces holes into $PbPdO_2$, with the values ranging between 150 $\mu$V K$^{-1}$ to 30 $\mu$V K$^{-1}$ at 300 K for small hole doping levels. In addition, as seen in the experimental data, that values at 600 K are substantially larger than those at 300 K. The trend and the magnitude of the values encourage the comparison with experiment, and suggest that even simple Boltzmann transport theory captures some of the physics in this system. To ensure that the results presented here are not excessively sensitive to the value of the Hubbard $U$ that was selected, we also performed calculations using $U_{eff} = 5$ eV, and found substantially similar results to the ones found for $U_{eff} = 3$ eV.

## Thermal conductivity and thermoelectric figure of merit

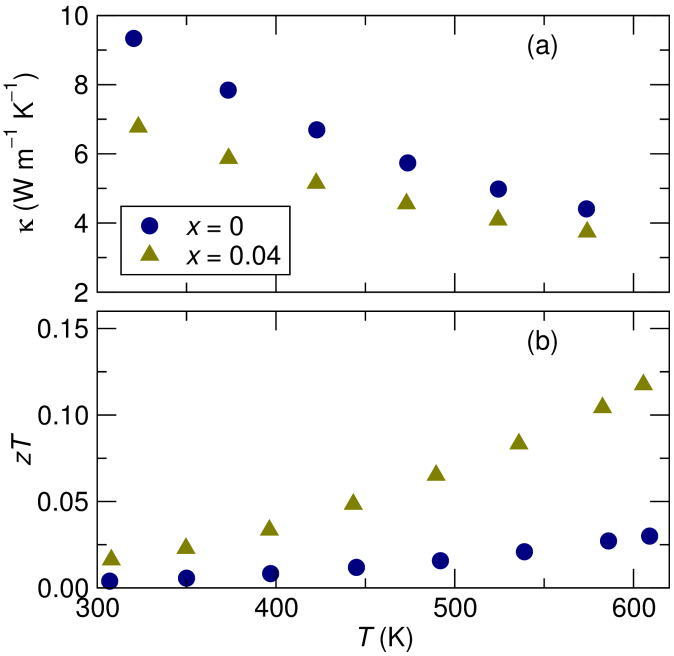


Figure 7: (a) Thermal conductivity and (b) $zT$ of $PbPd_{1-x}Li_xO_2$ samples obtained from the electrical and thermal transport measurements. The thermal conductivity of 4 W m$^{-1}$ K$^{-1}$ gives Li-substituted $PbPdO_2$ a $zT = 0.12$ at 600 K. Higher $zT$ values are anticipated as the temperature is further increased.

The thermal conductivities of stoichiometric $PbPdO_2$ and $PbPd_{0.96}Li_{0.04}O_2$ were measured from room temperature to 973 K. At the highest measured temperature of 973 K, the values for both samples approach 2.5 W m$^{-1}$ K$^{-1}$. Low thermal conductivity is expected

from the crystal structure, which consists of a layered arrangement of heavy Pb atoms, and potentially, lattice anharmonicity due to the lone pairs in an asymmetric coordination environment.[49] However, the measured values of the thermal conductivity are somewhat high for an effective thermoelectric. Applying the Wiedemann-Franz law, $\kappa_{el} = LT/\rho$, where $\kappa_{el}$ is the electronic contribution to thermal conductivity and $L$ is $2.44\times10^{-8}$ W Ω K$^{-2}$, we obtain a $\kappa_{el}$ of about 0.36 W m$^{-1}$ K$^{-1}$ for the Li-substituted sample at the highest temperature, leading to lattice thermal conductivities just greater than 2 W m$^{-1}$ K$^{-1}$. For example, at temperatures near 700 K, widely used thermoelectrics have values of lattice thermal conductivity below 1 W m$^{-1}$ K$^{-1}$.[4] The thermal conductivity can be combined with the electrical properties to give the thermoelectric figure of merit, $zT = S^2T/(\rho\kappa)$. Figure 7 shows the measured thermal conductivity and the resulting $zT$. The Li-substituted sample of $PbPdO_2$ has a $zT = 0.12$ at 600 K. It is clear that the peak $zT$ has not been reached and electrical measurements to higher temperature would yield even higher $zT$ values due to smaller thermal conductivities and larger Seebeck coefficients. In addition, single crystals of Li-substituted $PbPdO_2$ could show markedly decreased resistivities similar to what is seen in $Na_xCoO_2$ in which the resistivity at 800 K drops from $3.6\times10^{-3}$ Ω cm to $5.2\times10^{-4}$ Ω cm,[37] without significant effects on the Seebeck coefficient or thermal conductivity, and therefore yet higher values of $zT$.

# Conclusion

Li has been substituted for Pd in $PbPdO_2$, corresponding to hole doping. The Li substitution site and level of substitution have been established through Rietveld refinement of neutron diffraction data. The substitution limit appears to be close to 4 mol % Li substitution, beyond which evidence for further substitution is not observed. Metallic resistivities are reached with as little as 2 % Li substitution for Pd. The Seebeck coefficient of the substituted samples remains high, at $>100$ μV/K at room temperature and approaches 200 μV/K

at 600 K. Despite the relatively high lattice thermal conductivity of the compound, a $zT = 0.12$ is measured at 600 K. Similar electrical properties are observed in the high performing complex cobalt oxide compounds, arising from spin and orbital degeneracy, which are not present in Li-substituted $PbPdO_2$. Our findings suggest potentially new avenues to achieving high performing oxide thermoelectric materials, and encourage the search for such properties in oxides of more earth-abundant metals than the ones studied here.

## Acknowledgement

This work was supported by the National Science Foundation through DMR-1403862. R.P. and M.E.G. acknowledge support by the German Science Foundation within SFB/TR80, project G8. We thank Dr. Amanda Strom for help with various experimental aspects of this work, and acknowledge the preliminary work on this system by Phillip Barton and Rachel Beal. This work made use of the shared experimental facilities of the Materials Research Laboratory, supported by NSF MRSEC Program (DMR-1121053), and the Center for Scientific Computing at UCSB, supported by NSF MRSEC (DMR-1121053), NSF CNS-0960316 and Hewlett Packard. The Materials Research Laboratory is a member of the NSF-supported Materials Research Facilities Network.

## References

(1) Snyder, G. J.; Toberer, E. S. Complex Thermoelectric Materials. *Nat. Mater.* **2008**, *7*, 105–114.

(2) Walia, S.; Balendhran, S.; Nili, H.; Zhuiykov, S.; Rosengarten, G.; Wang, Q. H.; Bhaskaran, M.; Sriram, S.; Strano, M. S.; Kalantar-zadeh, K. Transition Metal Oxides – Thermoelectric Properties. *Prog. Mater. Sci.* **2013**, *58*, 1443–1489.

(3) Koumoto, K.; Wang, Y.; Zhang, R.; Kosuga, A.; Funahashi, R. Oxide Thermoelectric Materials: A Nanostructuring Approach. *Annu. Rev. Mater. Res.* **2010**, *40*, 363–394.

(4) Gaultois, M. W.; Sparks, T. D.; Borg, C. K. H.; Seshadri, R.; Bonificio, W. D.; Clarke, D. R. Data-Driven Review of Thermoelectric Materials: Performance and Resource Considerations. *Chem. Mater.* **2013**, *25*, 2911–2920.

(5) Terasaki, I.; Sasago, Y.; Uchinokura, K. Large Thermoelectric Power in $NaCo_2O_4$ Single Crystals. *Phys. Rev. B* **1997**, *56*, R12685–R12687.

(6) Okada, S.; Terasaki, I. Physical Properties of Bi-Based Rhodium Oxides with $RhO_2$ Hexagonal Layers. *Jpn. J. Appl. Phys.* **2005**, *44*, 1834–1837.

(7) Klein, Y.; Hébert, S.; Pelloquin, D.; Hardy, V.; Maignan, A. Magnetoresistance and Magnetothermopower in the Rhodium Misfit Oxide $[Bi_{1.95}Ba_{1.95}Rh_{0.1}O_4][RhO_2]_{1.8}$. *Phys. Rev. B* **2006**, *73*, 165121–1–165121–6.

(8) Kobayashi, W.; Hébert, S.; Pelloquin, D.; Pérez, O.; Maignan, A. Enhanced Thermoelectric Properties in a Layered Rhodium Oxide with a Trigonal Symmetry. *Phys. Rev. B* **2007**, *76*, 245102–1–245102–5.

(9) Ichikawa, S.; Terasaki, I. Metal-Insulator Transition in $Ca_{1-x}Li_xPd_3O_4$. *Phys. Rev. B* **2003**, *68*, 233101–1–233101–4.

(10) Taniguchi, T.; Nagata, Y.; Ozawa, T. C.; Sato, M.; Noro, Y.; Uchida, T.; Samata, H. Insulator–Metal Transition Induced in $Sr_{1-x}Na_xPd_3O_4$ for Small Na-Substitutions. *J. Alloys Compd.* **2004**, *373*, 67–72.

(11) Uriu, R.; Shimada, D.; Tsuda, N. Metal to Insulator Transition in $Pd_{1-x}$ $Li_xO$. *J. Phys. Soc. Japan* **1991**, *60*, 2479–2480.

(12) Ozawa, T. C.; Taniguchi, T.; Nagata, Y.; Noro, Y.; Naka, T.; Matsushita, A. Metal–Insulator Transition and Large Thermoelectric Power of a Layered Palladium Oxide: $PbPdO_2$. *J. Alloys Compd.* **2005**, *388*, 1–5.

(13) Meyer, V. H.; Muller-Buschbaum, H. A New Cross Linkage of Planar Polyhedra around $Pd^{2+}$ in $PbPdO_2$. *Z. Anorg. Allg. Chem.* **1978**, *442*, 26–30.

(14) Wang, X. L. Proposal for a New Class of Materials: Spin Gapless Semiconductors. *Phys. Rev. Lett.* **2008**, *100*, 156404–1–156404–4.

(15) Chen, S. W.; Huang, S. C.; Guo, G. Y.; Lee, J. M.; Chiang, S.; Chen, W. C.; Liang, Y. C.; Lu, K. T.; Chen, J. M. Gapless Band Structure of $PbPdO_2$: A Combined First Principles Calculation and Experimental Study. *Appl. Phys. Lett.* **2011**, *99*, 012103–1–012103–3.

(16) Kurzman, J. A.; Miao, M.-S.; Seshadri, R. Hybrid Functional Electronic Structure of $PbPdO_2$ , a Small-Gap Semiconductor. *J. Phys. Condens. Matter* **2011**, *23*, 465501–1–465501–7.

(17) Lee, K. J.; Choo, S. M.; Yoon, J. B.; Song, K. M.; Saiga, Y.; You, C.-Y.; Hur, N.; Lee, S. I.; Takabatake, T.; Jung, M. H. Magnetic Properties of Gapless Semiconductors: $PbPdO_2$ and $PbPd_{0.9}Co_{0.1}O_2$. *J. Appl. Phys.* **2010**, *107*, 09C306–1–09C306–3.

(18) Su, H. L.; Huang, S. Y.; Chiang, Y. F.; Huang, J. C. A.; Kuo, C. C.; Du, Y. W.; Wu, Y. C.; Zuo, R. Z. Unusual High-Temperature Ferromagnetism of $PbPd_{0.81}Co_{0.19}O_2$ Nanograin Film. *Appl. Phys. Lett.* **2011**, *99*, 102508–1–102508–3.

(19) Ozawa, T. C.; Taniguchi, T.; Nagata, Y.; Noro, Y.; Naka, T.; Matsushita, A. Cu Doping and Pressure Effect on a Layered Palladium Oxide: $PbPdO_2$. *J. Alloys Compd.* **2005**, *395*, 32–35.

(20) Rietveld, H. M. A Profile Refinement Method for Nuclear and Magnetic Structures. *J. Appl. Crystallogr.* **1969**, *2*, 65–71.

(21) Coelho, A. TOPAS Academic V5. 2013.

(22) Momma, K.; Izumi, F. *VESTA*: a Three-Dimensional Visualization System for Electronic and Structural Analysis. *J. Appl. Crystallogr.* **2008**, *41*, 653–658.

(23) Kieslich, G.; Birkel, C. S.; Douglas, J. E.; Gaultois, M.; Veremchuk, I.; Seshadri, R.; Stucky, G. D.; Grin, Y.; Tremel, W. SPS-Assisted Preparation of the Magneli phase $WO_{2.90}$ for Thermoelectric Applications. *J. Mater. Chem. A* **2013**, *1*, 13050–13054.

(24) Cowan, R. D. Pulse Method of Measuring Thermal Diffusivity at High Temperatures. *J. Appl. Phys.* **1963**, *34*, 926–927.

(25) Kresse, G.; Furthmüller, J. Efficiency of Ab-Initio Total Energy Calculations for Metals and Semiconductors Using a Plane-Wave Basis Set. *Comput. Mater. Sci.* **1996**, *6*, 15–50.

(26) Kresse, G.; Marsman, M.; Furthmüller, J. Vienna Ab-Initio Simulation Package: VASP the GUIDE. 2012.

(27) Blöchl, P. E. Projector Augmented-Wave Method. *Phys. Rev. B* **1994**, *50*, 17953–17979.

(28) Kresse, G.; Joubert, D. From Ultrasoft Pseudopotentials to the Projector Augmented-Wave Method. *Phys. Rev. B* **1999**, *59*, 1758–1775.

(29) Perdew, J. P.; Burke, K.; Ernzerhof, M. Generalized Gradient Approximation Made Simple. *Phys. Rev. Lett.* **1996**, *77*, 3865–3868.

(30) Curtarolo, S.; Setyawan, W.; Hart, G. L. W.; Jahnatek, M.; Chepulskii, R. V.; Taylor, R. H.; Wang, S.; Xue, J.; Yang, K.; Levy, O.; Mehl, M. J.; Stokes, H. T.; Dem-

chenko, D. O.; Morgan, D. AFLOW: An Automatic Framework for High-Throughput Materials Discovery. *Comput. Mater. Sci.* **2012**, *58*, 218–226.

(31) Setyawan, W.; Curtarolo, S. High-Throughput Electronic Band Structure Calculations: Challenges and Tools. *Comput. Mater. Sci.* **2010**, *49*, 299–312.

(32) Heyd, J.; Scuseria, G. E.; Ernzerhof, M. Hybrid Functionals Based on a Screened Coulomb Potential. *J. Chem. Phys.* **2003**, *118*, 8207–8215.

(33) Brgoch, J.; Lehner, A. J.; Chabinyc, M.; Seshadri, R. Ab Initio Calculations of Band Gaps and Absolute Band Positions of Polymorphs of $RbPbI_3$ and $CsPbI_3$: Implications for Main-Group Halide Perovskite Photovoltaics. *J. Phys. Chem. C* **2014**, *118*, 27721–27727.

(34) Madsen, G.; Singh, D. BoltzTraP. A Code for Calculating Band-Structure Dependent Quantities. *Comput. Phys. Commun.* **2006**, *175*, 67–71.

(35) Shannon, R. D. Revised Effective Ionic Radii and Systematic Studies of Interatomic Distances in Halides and Chalcogenides. *Acta Crystallogr. Sect. A* **1976**, *32*, 751–767.

(36) Brown, I. D.; Altermatt, D. Bond-Valence Parameters Obtained from a Systematic Analysis of the Inorganic Crystal Structure Database. *Acta Crystallogr. Sect. B* **1985**, *41*, 244–247.

(37) Fujita, K.; Mochida, T.; Nakamura, K. High-Temperature Thermoelectric Properties of $Na_xCoO_{2-\delta}$ Single Crystals. *Jpn. J. Appl. Phys.* **2001**, *40*, 4644–4647.

(38) Funahashi, R.; Matsubara, I. Thermoelectric Properties of Pb- and Ca-Doped $(Bi_2Sr_2O_4)_xCoO_2$ Whiskers. *Appl. Phys. Lett.* **2001**, *79*, 362–364.

(39) Shikano, M.; Funahashi, R. Electrical and Thermal Properties of Single-Crystalline $(Ca_2CoO_3)_{0.7}CoO_2$ with a $Ca_3Co_4O_9$ Structure. *Appl. Phys. Lett.* **2003**, *82*, 1851–1853.

(40) Heikes, R. R.; Ure, R. W. *Thermoelectricity: Science and Engineering*; Interscience Publishers, 1961.

(41) Koshibae, W.; Tsutsui, K.; Maekawa, S. Thermopower in Cobalt Oxides. *Phys. Rev. B* **2000**, *62*, 6869–6872.

(42) Koshibae, W.; Maekawa, S. Effects of Spin and Orbital Degeneracy on the Thermopower of Strongly Correlated Systems. *Phys. Rev. Lett.* **2001**, *87*, 236603–1–236603–4.

(43) Wang, Y.; Rogado, N. S.; Cava, R. J.; Ong, N. P. Spin Entropy as the Likely Source of Enhanced Thermopower in $Na_xCo_2O_4$. *Nature* **2003**, *423*, 425–428.

(44) Singh, D. J. Electronic Structure of $NaCo_2O_4$. *Phys. Rev. B* **2000**, *61*, 13397–13402.

(45) Takeuchi, T.; Kondo, T.; Takami, T.; Takahashi, H.; Ikuta, H.; Mizutani, U.; Soda, K.; Funahashi, R.; Shikano, M.; Mikami, M.; Tsuda, S.; Yokoya, T.; Shin, S.; Muro, T. Contribution of Electronic Structure to the Large Thermoelectric Power in Layered Cobalt Oxides. *Phys. Rev. B* **2004**, *69*, 125410–1–125410–9.

(46) Kuroki, K.; Arita, R. Pudding Mold Band Drives Large Thermopower in $Na_xCoO_2$. *J. Phys. Soc. Japan* **2007**, *76*, 083707–1–083707–4.

(47) Dudarev, S.; Botton, G.; Savrasov, S.; Humphreys, C.; Sutton, A. Electron-Energy-Loss Spectra and the Structural Stability of Nickel Oxide: An LSDA+U Study. *Phys. Rev. B* **1998**, *57*, 1505–1509.

(48) Gruner, M.; Eckern, U.; Pentcheva, R. Impact of Strain-Induced Electronic Topological Transition on the Thermoelectric Properties of PtCoO2 and PdCoO2. *Phys. Rev. B* **2015**, *92*, 235140–1–235140–10.

(49) Skoug, E. J.; Morelli, D. T. Role of Lone-Pair Electrons in Producing Minimum Thermal Conductivity in Nitrogen-Group Chalcogenide Compounds. *Phys. Rev. Lett.* **2011**, *107*, 235901–1–235901–5.

# Graphical TOC Entry